






Article

Biogenic Nanomagnetic Carriers Derived from Magnetotactic Bacteria: Magnetic Parameters of Magnetosomes Inside *Magnetospirillum* spp.

Vyacheslav Ryzhov ^{1,*}, Vladimir Deriglazov ¹, Denis Grouzdev ², Veronika Kozaieva ^{3,4}, Igor Kiselev ¹, Ivan Larionov ¹, Kamil Gareev ^{4,5}, Nikita Sitkov ^{4,5}, Tatiana Zimina ^{4,5}, Yaroslav Marchenko ¹ and Maxim Shevtsov ^{4,6,7,8,*}

- ¹ Petersburg Nuclear Physics Institute, National Research Centre “Kurchatov Institute”, 188300 Gatchina, Russia
- ² SciBear OU, Tartu mnt 67/1-13b, Kesklinna Linnaosa, 10115 Tallinn, Estonia
- ³ Research Center of Biotechnology of the RAS, Institute of Bioengineering, 119071 Moscow, Russia
- ⁴ Laboratory of Biomedical Nanotechnologies, Institute of Cytology of the RAS, 194064 St. Petersburg, Russia
- ⁵ Department of Micro and Nanoelectronics, Saint Petersburg Electrotechnical University “LETI”, 197376 St. Petersburg, Russia
- ⁶ Department of Radiation Oncology, Klinikum Rechts der Isar, Technical University Munich, 81675 Munich, Germany
- ⁷ Personalized Medicine Centre, Almazov National Medical Research Centre, 197341 St. Petersburg, Russia
- ⁸ Institute of Life Sciences and Biomedicine, Far Eastern Federal University, 690922 Vladivostok, Russia
- * Correspondence: ryzhov_va@pnpi.nrcki.ru (V.R.); maxim.shevtsov@tum.de (M.S.); Tel.: +49-173-1488882 (M.S.)



Citation: Ryzhov, V.; Deriglazov, V.; Grouzdev, D.; Kozaieva, V.; Kiselev, I.; Larionov, I.; Gareev, K.; Sitkov, N.; Zimina, T.; Marchenko, Y.; et al. Biogenic Nanomagnetic Carriers Derived from Magnetotactic Bacteria: Magnetic Parameters of Magnetosomes Inside *Magnetospirillum* spp. *Appl. Sci.* **2023**, *13*, 2431. <https://doi.org/10.3390/app13042431>

Academic Editor: Cristina Satriano

Received: 19 December 2022

Revised: 8 February 2023

Accepted: 11 February 2023

Published: 14 February 2023



Copyright: © 2023 by the authors. Licensee MDPI, Basel, Switzerland. This article is an open access article distributed under the terms and conditions of the Creative Commons Attribution (CC BY) license (<https://creativecommons.org/licenses/by/4.0/>).

Abstract: Magnetic parameters of magnetosomes inside the bacteria of MSR-1, LBB-42, AMB-1, SP-1, BB-1, and SO-1 strains of the genus *Magnetospirillum* fixed by 5% formalin in the nutrient medium were estimated by measurements of the nonlinear longitudinal response to a weak *ac* magnetic field (NLR-M2) at room temperature. For the BB-1, MSR-1, and AMB-1 strains, the measurements of the electron magnetic resonance (EMR) spectra with the special X-band spectrometer for wide-line registration were also carried out. To trace the evolution of the magnetic state of the magnetosomes during the long-term storage, freshly prepared samples (“new”) and samples after a year of storage at 4 °C (“old”) were studied. The assessment of the state of the bacteria ensemble in the medium after the long-term storage was carried out for one typical strain (BB-1) using atomic force microscopy. The stable single-domain state of magnetic centers in the magnetosomes indicating their proximity to a superparamagnetic (SPM) regime was found at the scan frequency 0.02 Hz of the steady magnetic field. This allowed a semi-quantitative analysis of M2 data to be carried out with the formalism based on the numerical solution of the kinetic Fokker–Planck equation for SPM particles. Processing the NLR-M2 data demonstrated the presence of two kinds of magnetosomes in both the “new” and “old” samples: (i) those with the large magnetic moment (the “heavy”, monodisperse mode) and (ii) those with the comparatively small magnetic moment (the “light”, highly dispersed mode). The EMR spectra were formed mostly by the “heavy” fraction for both samples. The presence of two peaks in the spectra evidenced the presence of conventional uniaxial magnetic anisotropy in the magnetosomes. The appearance of one or two additional peaks in the spectra in the “old” fraction of some strains implied their instability at the long-term storage, even when fixed by formalin and sealed in the nitrogen atmosphere.

Keywords: magnetosomes; *Magnetospirillum* spp.; nonlinear response to *ac* magnetic field; electron magnetic resonance

1. Introduction

Magnetotactic bacteria (MTB) are organisms that have been deeply studied in recent years, due to their interesting magnetic behavior and their potential applications in therapeutics and hyperthermia, and as biosensor devices. MTB produce organelles arranged as intracellular chains of submicron-sized membrane-enclosed magnetic particles called magnetosomes, composed of magnetite (Fe_3O_4) or greigite (Fe_3S_4) single crystals [1–5]. They orient and move along the Earth's geomagnetic field lines searching the areas of aqueous reservoirs where the magnetic field helps MTB to locate at the oxic–anoxic transition zone within chemical gradients.

The crystalline properties of magnetosomes make them very attractive for bioengineering applications, including use as contrast agents in nuclear magnetic resonance imaging or nano-heaters in hyperthermia therapy [6]. In the latter case, the heating efficiency demonstrated by magnetosomes was reported to be higher than the heating efficiency that characterized the nanoparticles prepared by the chemical synthesis protocols [7,8]. Since the competitive chemical procedures yield wide-range nanoparticle distributions [9,10] and smaller heating efficiencies, it became appealing to use MTB as bioreactors to produce high-quality magnetic nanoparticles for medical purposes. MTB of the genus *Magnetospirillum* are the best studied MTB, due to their relatively easy cultivation. *Magnetospirillum* spp. are basically spirilla-shaped bacteria, which produce magnetite-containing magnetosomes organized in a single chain [11]. Mature crystals have a truncated octahedral shape and an average diameter of 40–45 nm [12]. All *Magnetospirillum* species are chemoorganoheterotrophs and require microaerophilic conditions for magnetosome biosynthesis. Minor differences between species relate to the use of different sets of substrates and the range of the amount of oxygen in which cells can grow [11,13]. It was shown that model strains *Magnetospirillum magneticum* AMB-1 and *Magnetospirillum gryphiswaldense* MSR-1 have distinct strategies in the magnetosome chain organization. In AMB-1, the chain is fragmented, while in MSR-1, the magnetic crystals are arranged as a continuous chain [14–16]. The magnetosome size and the amount of magnetosomes in the chains depend on the stage of growth [17]. In addition, physical properties, including magnetic ones, are influenced by the growth conditions and the composition of the medium [18–22].

Despite a large amount of information accumulated on the magnetic behavior of MTB [9,23,24], there is still lack of information concerning the magnetic parameters (primarily static as well as dynamic) of magnetosomes inside the cells of different *Magnetospirillum* species. Therefore, the main purpose of this study was to investigate freshly grown magnetotactic spirilla strains of the genus *Magnetospirillum* that were then fixed with 5% formalin in comparison with strains that were grown and fixed a year before, to estimate the magnetic parameters of the magnetosomes inside the cells and to trace their time evolution in the nutrient medium via adding 5% formalin.

In magnetic measurements, we employed a nonlinear longitudinal response to a weak *ac* field with the registration of the second harmonic of magnetization M_2 (NLR-M2). The recorded dependences of the M_2 phase components on the static magnetic field H were further processed using formalism based on the Gilbert–Landau–Lifshitz equation for the stochastic dynamics of superparamagnetic (SP) particles underlying the Fokker–Planck (FP) kinetic equation [25,26]. This allowed us to estimate the magnetic parameters of the magnetosomes, to establish their two-mode distribution over magnetic moments, and, accordingly, to determine their sizes, and to compare the results for some strains with electron magnetic resonance (EMR), atomic force microscopy (AFM), and known transmission electron microscopy (TEM) data.

2. Materials and Methods

2.1. Cultivation of MTB

M. moscoviense BB-1 [13], *M. gryphiswaldense* MSR-1 [27], and *M. caucaseum* SO-1 [13] were grown in a flask standard medium (FSM) [28] with 20 μM of Fe(III) citrate. *M. magneticum* AMB-1 [29], *M. marisnigri* SP-1 [13], and *M. kuznetsovii* LBB-42 [12] were grown

in a magnetic spirillum growth medium (MSGM) [30] with 20 μM of Fe(III) citrate. After 120 h of cultivation, a part of the bacteria was fixed by adding 5% formalin to the nutrient medium, while another part was used as grown. Both batches of the “new” bacteria in the nitrogen atmosphere were placed in sealed cuvettes for magnetic measurements and stored at 4 °C. To determine how well magnetosomes are preserved during long-term storage, the magnetic measurements were also carried out on the “old” bacteria after a year of storage under the same conditions.

2.2. Characterization of Bacteria

By using AFM, we characterized the state of the formalin-fixed *M. moscoviense* BB-1 strain and its magnetosomes after the long-term storage. The bacteria were imaged using a Scanning Probe Microscope (SPM) Solver manufactured by NT-MDT, Nova v. 1.0.26. The NSG03 (non-contact silicon gold-plated) probe was used with a tip radius of 10 nm and a height of 14–16 μm . The cantilever had a length of 135 μm , a width of 30 μm , and a thickness of 1.54 μm , while the force constant and the resonant frequency were 1.74 N/m and 90 kHz, respectively. The sample was prepared as follows: 5 microliters of the suspension were brought on a glass slide and dried for two minutes. The dried sample was immediately placed on the SPM table for scanning.

Transmission electron microscopy (TEM) was used to analyze the cell and magnetosome morphology. A drop of concentrated cells was placed on a formvar-carbon-coated copper grid, rinsed three times with MQ and dried in air. Bacteria imaging was carried out on a JEOL JEM-1011 (JEOL, Tokyo, Japan) transmission electron microscope with accelerating voltages of 80 kV.

2.3. Magnetic Measurements and Data Quantifying

Magnetosomes in *Magnetospirillum* spp. reveal large magnetic moments [5] that provide for the magnetization of the bacteria ensemble in a weak magnetic field to be close to saturation [31] and, hence, strong non-linearity of its $M(H)$ dependence [26]. To assess their magnetic parameters, the registration of the second harmonic of magnetization M_2 in the bacteria ensemble under the steady magnetic field H and the parallel weak ac field $h(t) = h \sin(\omega t)$ with $h = 1.1$ kA/m and $f = \omega/2\pi = 15.7$ MHz was performed. This approach provided for the elimination of the contribution from the diamagnetic environment (unlike SQUID measurements) and for a negligible contribution from possible paramagnetic centers in the bacteria (due to an almost linear character of their $M(H)$ dependence).

A homemade installation described earlier [32], adapted for studying MNPs [26,33,34], was used in experiments. It consisted of two dc -field Helmholtz coils, a radiofrequency (RF) generator with a low-frequency filter at the output, a two-mode (f , $2f$) resonant sensor containing the sample, and a receiver registering the second-harmonic response with a high-frequency filter at the input. High sensitivity of the setup was provided by (i) the use of the two-mode sensor, (ii) the effective record of the $2f$ signal induced by the sample with the $2f$ -mode selective system, (iii) deep suppression of the $2f$ voltage from the RF generator and the f voltage at the input of the receiver by the high- and low-frequency filters, respectively, ensuring the amplitudes of the ac field up to 4 kA/m, and (iv) the employment of materials and elements in the two-mode sensor which do not generate the spurious $2f$ signal. The Q -factor of the $2f$ mode $Q_2 \approx 200$ ensured the enhancement of the setup sensitivity by a factor of $\sqrt{Q_2}$ compared to the nonresonance registration in the ac susceptibility measurements.

Both signal components, $\text{Re}M_2(H, T)$ and $\text{Im}M_2(H, T)$, were recorded simultaneously as functions of H at room temperature, which corresponds approximately to the bacteria habitat temperature. The sample temperature was stabilized by a flow thermostat using evaporated N_2 . The steady field H was slowly scanned in the range from -24 to 24 kA/m and backwards symmetrically relative to the point $H = 0$, with the scan frequency varied in the range of $8 \geq F_{sc} \geq 0.02$ Hz, to control the field hysteresis in the signal. In accordance with the symmetry properties of M_2 , the hysteresis provides evidence for the presence of a

ferromagnetic moment in the sample [35]. In the current experiments, the condition $M_2 \sim h^2$ was obeyed, which provided applicability of the analytical expressions for the M_2 response obtained by the perturbation theory [35,36] in the qualitative analysis of the experimental data. This technique was employed previously for studying biogenic MNPs in viable eukaryotic cells where a small amount of magnetosome-like structures was detected [37]. It is interesting to note that this response depended on the aggregation (suspension/pellet) of the cells. The sensitivity of the measurements was about $10^{-13} \text{ A}\cdot\text{m}^2$.

The measured dependences $\text{Re}M_2(H, T)$ and $\text{Im}M_2(H, T)$ were processed using the formalism of the numerical solution for the kinetic FP equation for the stochastic magnetization dynamics of superparamagnetic (SPM) particles with arbitrary directions of anisotropy axes [25],

$$2\tau_N \frac{\partial W}{\partial t} = -\frac{1}{\sin \vartheta} \left[\frac{\partial}{\partial \vartheta} (\tilde{J}_\vartheta \sin \vartheta) + \frac{\partial}{\partial \varphi} \tilde{J}_\varphi \right], \tag{1}$$

with

$$\tilde{J}_\vartheta = -\left[\beta \left(\frac{\partial \mathcal{H}}{\partial \vartheta} - \frac{1}{\alpha \sin \vartheta} \frac{\partial \mathcal{H}}{\partial \varphi} \right) W + \frac{\partial W}{\partial \vartheta} \right], \tag{2}$$

$$\tilde{J}_\varphi = -\left[\beta \left(\frac{1}{\alpha} \frac{\partial \mathcal{H}}{\partial \vartheta} + \frac{1}{\sin \vartheta} \frac{\partial \mathcal{H}}{\partial \varphi} \right) W + \frac{1}{\sin \vartheta} \frac{\partial W}{\partial \varphi} \right]. \tag{3}$$

Here, $W(t)$ is the nonequilibrium probability–density function for directions of the particle magnetic moment \mathbf{m} with the damping constant α and the time scale τ_N being the Néel free-diffusion (zero-potential) relaxation time proportional to α^{-1} and $\beta = 1/k_B T$. The magnetic potential \mathcal{H} consists of the *uniaxial* anisotropy energy and the energy of the magnetic moment in the total magnetic field $\mathbf{H} = \mathbf{H}_0 + \mathbf{h}$:

$$\mathcal{H} = -\frac{E_a}{m^2} (\mathbf{m}\mathbf{n})^2 - \mathbf{m}\mathbf{H},$$

where \mathbf{n} is the anisotropy axis direction. The direction of \mathbf{m} defined by the spherical angles ϑ and φ thermally fluctuates in the field \mathbf{H} (Figure 1).

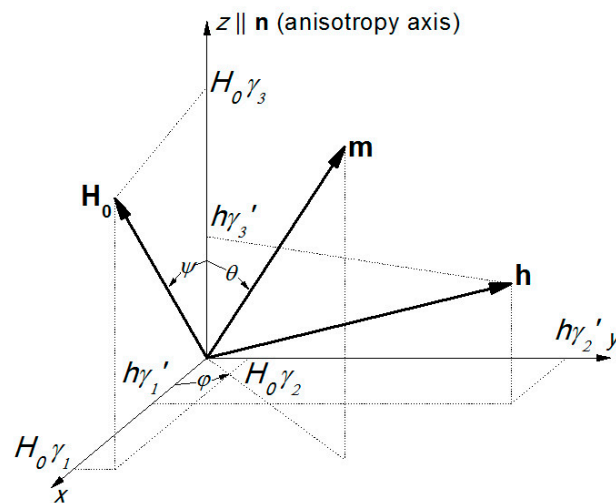


Figure 1. Magnetic field geometry.

The function $W(t)$ is expanded in the series on spherical harmonics

$$W(t, \vartheta, \varphi) = \sum_{lm} c_{lm}(t) Y_{lm}(\vartheta, \varphi), \tag{4}$$

and in the Fourier series reducing Equation (1) to a set of linear equations which, in turn, is expressed as a continuous-fraction matrix equation

$$\mathbf{S}_n = -[\mathbf{Q}_n + \mathbf{Q}_n^+ \mathbf{S}_{n+1} \mathbf{Q}_{n+1}]^{-1}, \tag{5}$$

with the matrices \mathbf{Q}_n , \mathbf{Q}_n^+ and \mathbf{Q}_{n+1} ($n = 1, 2, \dots$) composed of the spherical harmonics indices, the direction cosines γ_i and γ'_i of the magnetic fields relative to the anisotropy axis \mathbf{n} (Figure 1), as well as of the parameters entering Equations (1)–(3) and the magnetic potential \mathcal{H} . The normalized k th Fourier harmonic of the magnetic moment in the field direction is

$$m_k(\omega) = \sqrt{\frac{4\pi}{3}} \left[\gamma_3 c_{10}^k(\omega) + \frac{(\gamma_1 + i\gamma_2)c_{1-1}^k(\omega) - (\gamma_1 - i\gamma_2)c_{11}^k(\omega)}{\sqrt{2}} \right], \tag{6}$$

where $c_{ij}^k(\omega)$ are the Fourier transforms of $c_{lm}(t)$ in Equation (4). The quantities $c_{ij}^k(\omega)$ are the elements of the column vector \mathbf{S}_1 , the solution of Equation (5). The complex fit function for the M_2 response is obtained by the convolution of $m_k(\omega)$ for $k = 2$ with the distribution over the values of magnetic moments f_M :

$$M_2(H_0) = \tilde{M} \int f_M m_2(\omega, h, H_0) dM, \tag{7}$$

where \tilde{M} is the total saturation magnetization of the sample. The function f_M corresponds to the distribution over the particle volumes when all the particles are magnetically homogeneous with the same, size-independent magnetization. In most cases, the log-normal distribution is valid.

Computation of the fit function (7) at each experimental point requires multiple solving of Equation (5). The solution accuracy is determined by the retained terms in the spherical harmonics and Fourier expansions. The simultaneous fitting of the real and imaginary parts of the measured signals using Equation (7) yields the following quantities: (i) the sample saturation magnetization \tilde{M} , (ii) the mean magnetic moment M_C and the width of the f_M distribution σ , (iii) the mean anisotropy energy E_a and field H_a , (iv) the average angle Ψ between \mathbf{n} and \mathbf{H} (Figure 1), and (v) the parameters defining magnetization dynamics, viz., the damping constant α and the Néel relaxation time τ_N . Given the concentration of iron, additional information can be extracted, namely, the mass and volume saturation magnetizations of the sample, the average number of iron ions in the particles, the mean particle size, and some others.

This is a rather general approach. In particular, the requirement $h \ll H$ on the alternating magnetic field is not mandatory, thereby keeping the formalism valuable even for quite small H .

The formalism was applied to study a colloidal aqueous solution of SPM iron oxide nanoparticles in the dextran shell (SPIONs) [26]. The criterion of applicability of the procedure is the absence of, or the presence of only a small of, magnetic hysteresis in the H dependences of the signals, which points on the SPM nature of the response. The computational resources of the PIK Data Centre of NRC “Kurchatov Institute” (PNPI, Gatchina, Russia) were used, with the in-house provided software.

Prior to the fitting, the raw data were averaged between the direct (I_{dir}) and reverse (I_{rev}) scans and the part that was antisymmetric relative to $H = 0$ was extracted, as required by the model, as follows:

$$I_{av} = \frac{1}{4} [I_{dir}(H) + I_{rev}(H) - I_{dir}(-H) - I_{rev}(-H)]. \tag{8}$$

This averaging removed a possible constant bias to obey the condition $\text{Re}M_2(H = 0) = 0$ required by the formalism and reduced the data to the region $H > 0$ to use in the data-

fit procedure. In addition, as the magnetosomes in the specimens were disoriented, the isotropic distribution of the anisotropy axes directions was implied.

A set of parameters characterizing the magnetosome ensembles in the bacteria under study was obtained, describing their magnetic properties, such as the magnetic moments, the magnetic anisotropy energy, and the saturation magnetization. The most relevant parameter for the assessment of the magnetosome state is the number of magnetically active centers in each bacteria line derived as the ratio of the saturation magnetization and the magnetic moment.

To obtain additional information on the magnetic state of the magnetosomes, we used EMR. We applied a special homemade X-band spectrometer operating at the frequency $F = \omega/2\pi = 8.54$ GHz [38]. The spectrometer was supplied with a cylindrical two-mode balanced microwave resonator with the TE₁₁₁ type of electromagnetic oscillations. The *dc* magnetic field \mathbf{H} was directed along the cylinder *z* axis. The sample (MTB in the cultivation medium with the addition of formalin for the bacteria fixation) was placed at the bottom of the resonator in the special cylindrical cavity, where it was affected by the *ac* field \mathbf{h} linearly polarized along the *x* axis perpendicular to \mathbf{H} (the excitation *xz* plane). The detection *yz* plane was perpendicular to the excitation one, and thus the detected signal was proportional to the off-diagonal component of the susceptibility tensor $\chi_{yx}(\omega)$ corresponding to the *y* component of the induced magnetic moment $M_y(\omega) = \chi_{yx}(\omega)h_x(\omega)$. Deep frequency-independent decoupling between the excitation and detection modes was achieved by ensuring the frequency degeneracy, viz., the independence of the eigenfrequencies of the resonator from the rotation of the excitation plane around the *z* axis in the *xy* plane of the resonator. This made it possible to use a microwave source with the high oscillation power ~1 W without frequency and amplitude noises at the detector input which, in turn, provided the possibility of not using the field modulation technique and enhancing the spectrometer sensitivity in registering broad EMR lines. This facility has proved its efficiency in a number of condensed matter studies, including aqueous and buffer colloidal solutions of MNPs [26,34–37,39,40].

This technique is also expected to provide the estimation of the dipolar coupling energy of magnetosomes in the chain directly inside the cells.

3. Results and Discussion

3.1. Transmission Electron Microscopy

As mentioned above, *Magnetospirillum* spp. forms one chain of magnetosomes used for orientation in the Earth's magnetic field, as shown in Figure 2 for *M. caucaseum* SO-1 and *M. marisnigri* SP-1 strains. The amount of magnetosomes in the chain, as well as their size, differs in different *Magnetospirillum* spp. strains [1–5]. BB-1, SO-1, SP-1, MS-1, and LBB-42 produce ~25 magnetosomes per cell with an average size of 40–50 nm; AMB-1 produces ~20 magnetosomes per cell with the size ~45 nm; MSR-1 produces ~30 magnetosomes with the size 32–45 nm.

3.2. Atomic Force Microscopy

The AFM image of the *M. moscoviense* BB-1 “old” prepared in the manner described above is shown in Supplement Figure S1. Magnetosome aggregates and chains of various lengths and configurations, as well as single magnetosomes from destroyed cells of the BB-1 strain, are visible in the field of the Figure. Preserved BB-1 cells can be expected to contain such fragments, as well as intact and partially destroyed magnetosome chains. It can also be expected that a part of the ensemble of the BB-1 bacteria includes formalin-fixed cells at the stage of division, containing halves of the mature chains of magnetosomes.

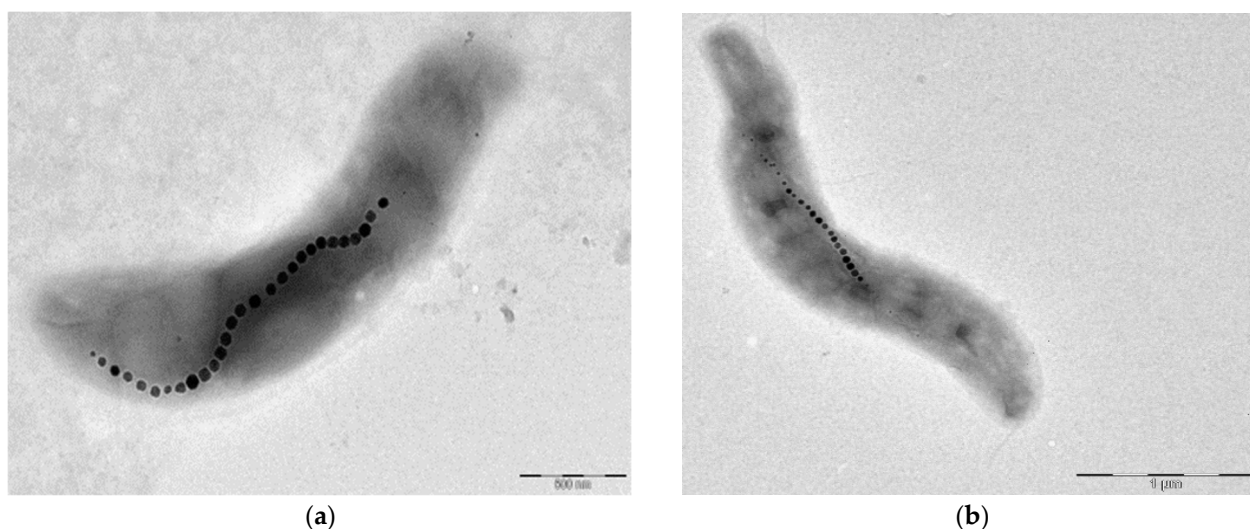


Figure 2. TEM images of *M. caucaseum* SO-1 (a) and *M. marisnigri* SP-1 (b) with a chain of magnetosomes.

3.3. NLR-M2 Results

To determine the magnetic parameters of magnetosomes inside the bacteria (without their destruction) in freshly grown cultures without fixation with formalin and in the medium with the addition of formalin for fixation, 1-mL cuvettes were used, filled, and sealed in the nitrogen atmosphere. The experiments were carried out at room temperature.

To characterize the magnetosome magnetic state (single-domain/multi-domain), the dependences $\text{Re}M_2(H)$ and $\text{Im}M_2(H)$ were registered at three steady field scanning frequencies $F_{sc} = 8, 0.25,$ and 0.02 Hz. The increase in the scanning period provides more time for the relaxation of magnetization. The dependence of the magnetic hysteresis on the scan frequency would indicate its dynamic character, suggesting the stable single-domain state of magnetosomes and the presence of magnetic anisotropy [31,34,36,41]. The absence of such dependence, in contrast, would indicate the formation of multidomain aggregates due to the adhesion of the magnetosomes after the destruction of their lipid shells. The magnetic relaxation in this case is determined by the motion of the domain walls [31,41] rather than by the rotation of the nanoparticle magnetic moment. The hysteresis in this case is associated with the pinning of the magnetic moment on structural inhomogeneities and does not depend on the time allotted for relaxation (the scanning period of the field H).

The phase components $\text{Re}M_2(H)$ and $\text{Im}M_2(H)$ recorded at $F_{sc} = 8$ and 0.25 Hz, as well as $\text{Re}M_2(H)$ recorded at $F_{sc} = 0.02$ Hz (the latter together with their best fit) for some strains (MSR-1, AMB-1, LBB-42, and SP-1), both for the “old” and “new” bacterial samples, are shown in Figures 3–6.

As was found in the NLR-M2 measurements, the addition of 5% formalin to the as-grown cultures in the medium does not lead to a detectable change in the M_2 response in five days, except for the MSR-1 strain (not shown). This implies only a weak influence of such a concentration of formalin on the internal organization of magnetosomes in the cells for most of the strains, at least during this time interval. As for the MSR-1 strain, in five days after the formalin administration, the amplitude of the M_2 response grew approximately two-fold in both phase components, accompanied by a considerable increase in the field hysteresis, indicating some unexpected tendency for this strain. From Figure 3, this tendency persists for a longer storage period. However, it is much less pronounced with a lower scan frequency, as seen from the ratio of the signals in panels (c) and (f) compared to that in the panels (a) and (d).

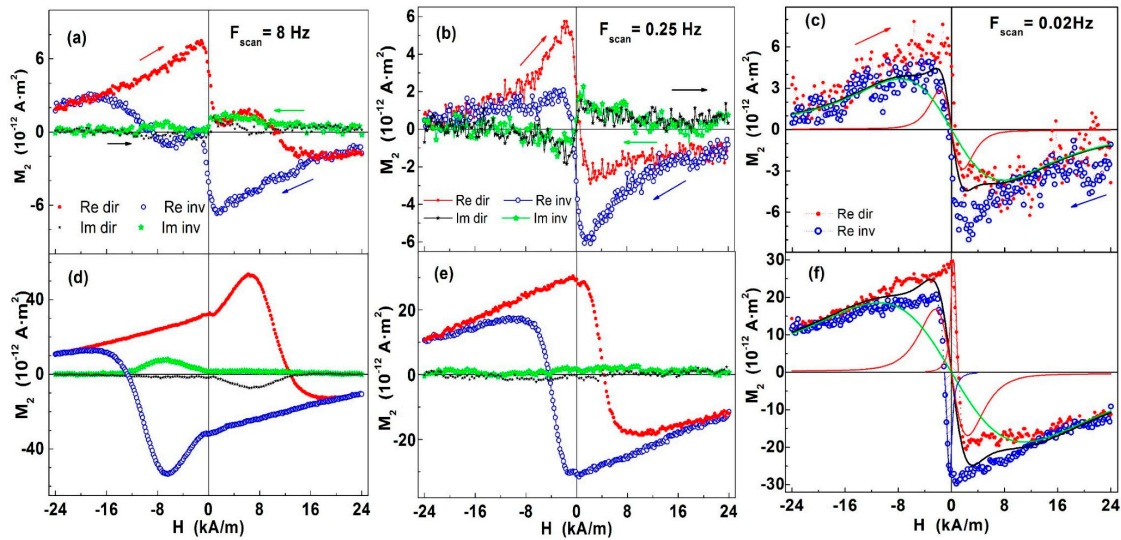


Figure 3. Dependences on static field H of phase components of M_2 response, $\text{Re}M_2(H)$ (open blue and solid red circles) and $\text{Im}M_2(H)$ (open green and solid black stars), for MSR-1 strain recorded at frequencies of H -scan $F_{sc}=8$ and 0.25 Hz are presented in panels (a,b,d,e). Solid symbols present the curves recorded at direct H -scan and open symbols are used for curves registered at the reverse sweep. For clarity, this is additionally indicated by arrows having the same color as the color of the corresponding symbols. Panels (c,f) display $\text{Re}M_2(H)$ dependences registered at $F_{sc}=0.02$ Hz and their best fits (black lines). Red and green lines correspond to two components of entire signal (see text). The upper panels (a,b,c) reflect the magnetic state of “fresh” (“new”) bacteria and lower panels (d,e,f) characterize the state of bacteria after one year of storage (“old”). The hatched peaks in (f) present M_2 response simulated for the NPs 40 nm size.

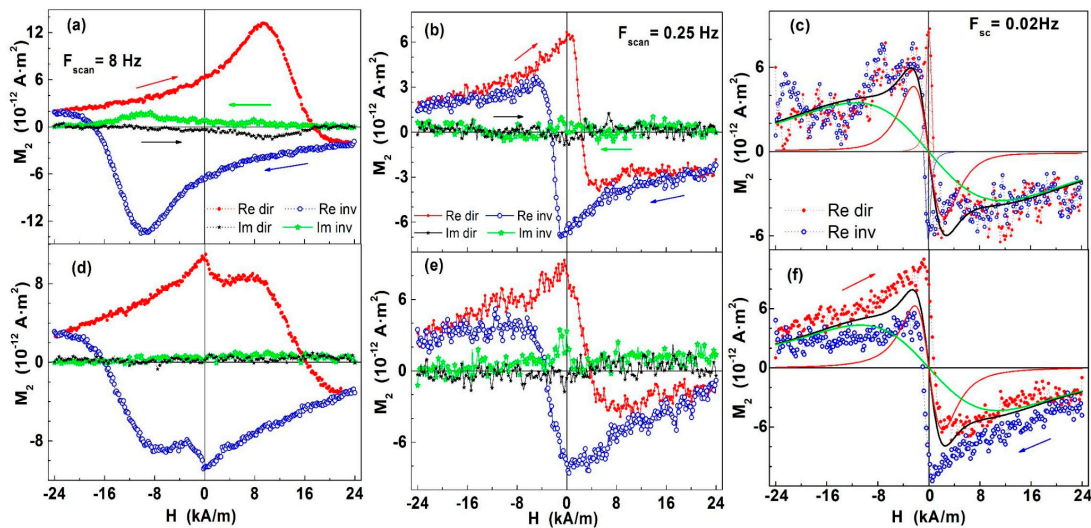


Figure 4. Dependences on static field H of phase components of M_2 response, $\text{Re}M_2(H)$ (open blue and solid red circles) and $\text{Im}M_2(H)$ (open green and solid black stars), for LBB-42 strain recorded at frequencies of H -scan $F_{sc}=8$ and 0.25 Hz are presented in panels (a,b,d,e). Solid symbols present the curves recorded at direct H -scan and open symbols are used for curves registered at the reverse sweep. For clarity, this is additionally indicated by arrows having the same color as the color of the corresponding symbols. Panels (c,f) display $\text{Re}M_2(H)$ dependences registered at $F_{sc}=0.02$ Hz and their best fits (black lines). Red and green lines correspond to two components of entire signal (see text). The hatched peaks in (f) present M_2 response simulated for the NPs 40 nm size.

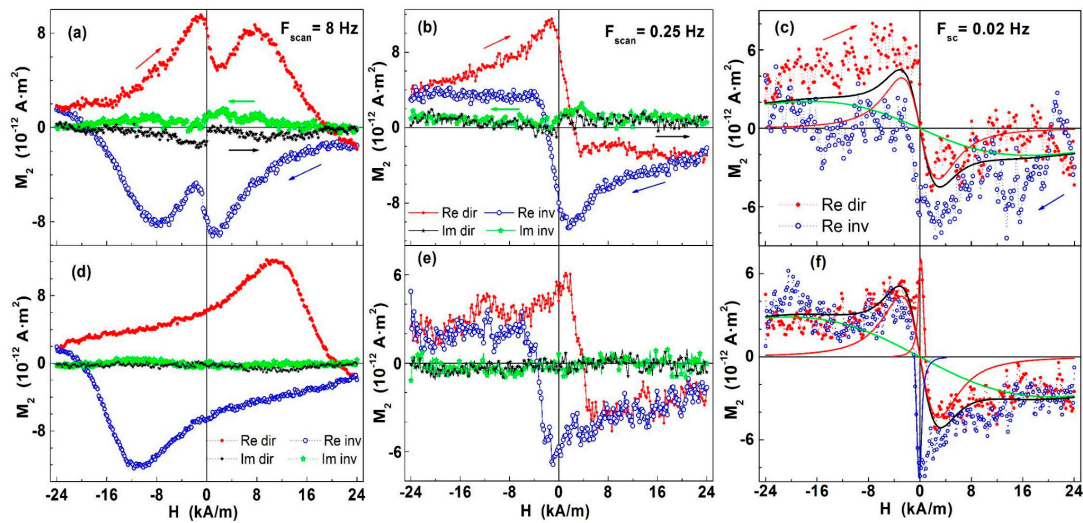


Figure 5. Dependences on static field H of phase components of M_2 response, $\text{Re}M_2(H)$ (open blue and solid red circles) and $\text{Im}M_2(H)$ (open green and solid black stars), for AMB-1 strain recorded at frequencies of H -scan $F_{\text{scan}} = 8$ and 0.25 Hz are presented in panels (a,b,d,e). Solid symbols present the curves recorded at direct H -scan and open symbols are used for curves registered at the reverse sweep. For clarity, this is additionally indicated by arrows having the same color as the color of the corresponding symbols. Panels (c,f) display $\text{Re}M_2(H)$ dependences registered at $F_{\text{scan}} = 0.02$ Hz and their best fits (black lines). Red and green lines correspond to two components of entire signal (see text). The upper panels (a–c) reflect the magnetic state of “fresh” (“new”) bacteria and lower panels (d–f) characterize the state of bacteria after one year of storage (“old”). The hatched peaks in (f) present M_2 response simulated for the NPs 40 nm size.

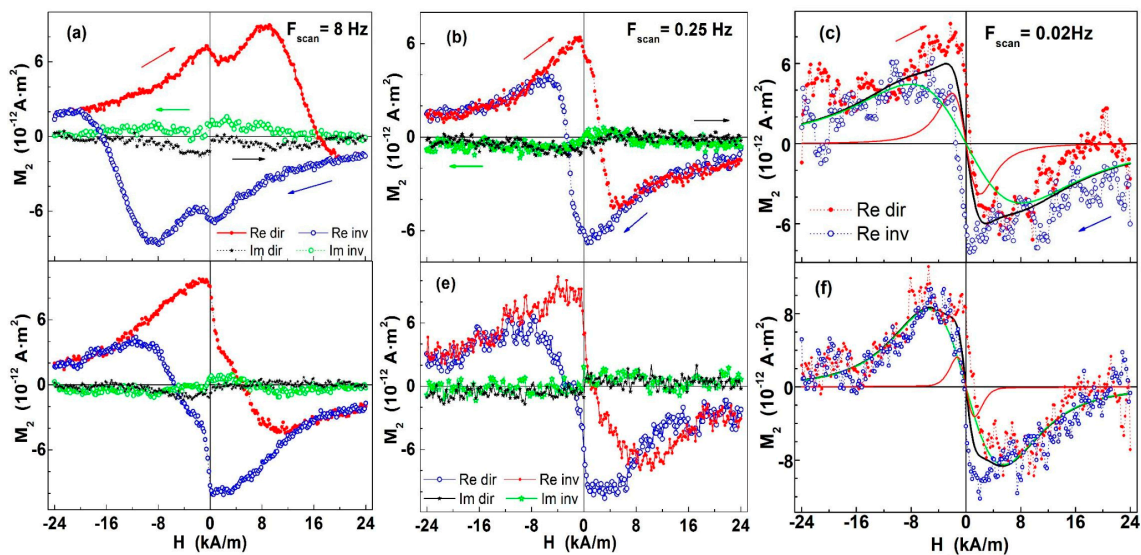


Figure 6. Dependences on static field H of phase components of M_2 response, $\text{Re}M_2(H)$ (open blue and solid red circles) and $\text{Im}M_2(H)$ (open green and solid black stars), for SP-1 strain recorded at frequencies of H -scan $F_{\text{scan}} = 8$ and 0.25 Hz are presented in panels (a,b,d,e). Solid symbols present the curves recorded at direct H -scan and open symbols are used for curves registered at the reverse sweep. For clarity, this is additionally indicated by arrows having the same color as the color of the corresponding symbols. Panels (c,f) display $\text{Re}M_2(H)$ dependences registered at $F_{\text{scan}} = 0.02$ Hz and their best fits (black lines). Red and green lines correspond to two components of entire signal (see text). The upper panels (a–c) reflect the magnetic state of “fresh” (“new”) bacteria and lower panels (d–f) characterize the state of bacteria after one year of storage (“old”).

As shown in Figures 3–6, the 8 Hz M_2 response exhibits a large field hysteresis. Decreasing the hysteresis with the scan frequency suggests its dynamical nature and the stable single-domain state of the magnetosomes. The vanishing of the hysteresis at $F_{sc} = 0.02$ Hz indicates proximity of the magnetosome ensemble to the SPM regime, opening the possibility of using the FP formalism. The imaginary component of the response coming from high-frequency magnetization dynamics [34–36] is significantly smaller than the real component. Our fitting of the M_2 response, taking into account the imaginary component, yielded the Gilbert damping factor of the order 10. Therefore, only the real part of the response was processed further, without taking into account the $\text{Im}M_2$ component.

The signals registered at $F_{sc} = 8$ Hz exhibited two peaks, indicating two fractions in the distribution of magnetic moments. Two peaks, somewhat less pronounced, were also present in the responses recorded at $F_{sc} = 0.25$ Hz. Therefore, when fitting the 0.02 Hz $\text{Re}M_2$ signals, we assumed a two-mode distribution of magnetic moments. It should be noted that the use of a single-mode model, even with the size dispersion, yields a much worse fit convergence, with a much larger chi-square. The synthesis of magnetosomes and their chains in MTB is genetically controlled [1–5,42,43], which suggests identity of their magnetic moments. The attempt to fit the first, larger-moment (“heavy”), mode with the dispersed moment distribution resulted, as a rule, in much worse fit quality. At the same time, it can be assumed that the second (“light”), mode, corresponding to a smaller average moment of the magnetic centers, can have a distribution in sizes and, accordingly, in magnetic moments. However, its account for the second mode does not yield regularly better chi-squares, and the moment distribution cannot be specified, due to the strong correlation between the fit parameters. The fit curves for the experimental data are presented in panels (c) and (f) of Figures 3–6. The contribution of the “heavy” fraction (red line) to the response is concentrated mainly in the weak-field region, while the contribution of the “light” fraction (green line) extends over the entire measured field region. Specifically, the rapid rise of the signal at low fields comes from the former, while the “tail” of the signal is formed by the latter.

The obtained parameters, viz., the saturation magnetization, the number of magnetic centers responsible for the signal, and the magnetic moment of the center, are shown in Table 1 for all the strains, each measured both as-prepared and after one year of storage. The anisotropy energies were also obtained from the data processing. However, their values seem to be controversial and not sufficiently reliable to be presented. At the moment, we provide only estimation of the order of their magnitude, $E_a \sim 10^3$ K.

Table 1. Magnetosome parameters obtained by fitting NLR-M2 experimental data from *Magnetospirillum* strains recorded at H -field scan frequency 0.02 Hz.

| Culture | | “Heavy” Fraction | | | “Light” Fraction | | |
|---------|-----|---|------------------|--------------------------|--|---------------------|--------------------------|
| | | \tilde{M} (10^{-10} A · m ²) | N_p (10^8) | M_C (10^5 μ_B) | \tilde{M} (10^{-8} A · m ²) | N_p (10^{10}) | M_C (10^5 μ_B) |
| BB-1 | old | 8.60 (46) | 4.45 (28) | 2.08 (7) | 4.19 (29) | 15.6 (1.3) | 0.289 (13) |
| | new | 5.9 (1.8) | 6.3 (2.2) | 1.01 (18) | 1.8 (4.4) | 14 (41) | 0.14 (21) |
| MSR-1 | old | 12.5 (7) | 9.6 (6) | 1.394 (46) | 2.45 (14) | 7.4 (5) | 0.357 (14) |
| | new | 1.176 (48) | 0.596 (29) | 2.128 (53) | 0.3069 (45) | 0.670 (11) | 0.4936 (41) |
| LBB-42 | old | 3.14 (37) | 1.79 (24) | 1.89 (12) | 0.55 (6) | 1.63 (22) | 0.366 (28) |
| | new | 3.25 (9) | 2.47 (8) | 1.421 (23) | 0.576 (10) | 2.124 (42) | 0.2926 (27) |
| AMB-1 | old | 3.91 (33) | 3.03 (29) | 1.39 (7) | 0.94 (11) | 4.3 (6) | 0.235 (13) |
| | new | 3.1 (7) | 2.3 (6) | 1.46 (18) | 0.6 (5) | 2.9 (3.0) | 0.23 (13) |
| SP-1 | old | 0.50 (15) | 0.15 (1.5) | 3.5 (34) | 0.2039 (38) | 0.251 (5) | 0.875 (10) |
| | new | 1.65 (39) | 0.87 (23) | 2.04 (25) | 0.344 (24) | 0.79 (7) | 0.467 (27) |
| SO-1 | old | 0.292 (25) | 0.082 (8) | 3.84 (20) | 0.297 (11) | 1.105 (46) | 0.290 (6) |
| | new | 9 (11) | 12 (3000) | 0 (200) | 0 (0.18) | 0 (3.9) | 0.05 (37) |

The large error bars in the obtained parameters, especially in the saturation magnetization and the number of magnetic centers, are due, on the one hand, to a poor signal-to-noise ratio at a given scan frequency and, on the other hand, to a strong correlation of the model parameters.

Note that we studied unsynchronized cell cultures in the aqueous suspension form, so the samples contained the cells at different stages of growth, including cells in the stage of division and dying cells. Thus, the ensemble of magnetosomes in the sample included the chains of magnetosomes of different sizes [17]. A contribution to the magnetic response was also made by the proteins containing iron nanoparticles, for the genetically controlled growth of the magnetosomes [44]. Unlike conventional magnetic measurements using dehydrated fixed samples, in our case of an aqueous solution, cells and magnetosomes can move and rotate. In particular, the scanning magnetic field H forces the cells with the magnetosome chain attached to the membrane to orient themselves along the field and to overturn when the field direction changes. The scan period $1/F_{sc} = 125$ ms is too short for the complete reversal. Therefore, the extremum of the $ReM_2(H)$ signal recorded, for example, at the reverse H scan is located in the quadrant $H > 0$, rather than in the quadrant $H < 0$ as expected for symmetrical reasons (Figures 3a,d, 4a,d, 5a,d and 6d). Increasing the sweep period to 4 s allows the cells to make such an overturn, although a certain time lag from the field, manifesting itself in the H hysteresis, still remains (Figures 3b,e, 4b,e, 5b and 6b,e). A short delay is observed even for the minimal $F_{sc} = 0.02$ Hz, which indicates that it takes time, even more than 50 s, to flip the cells.

From Table 1, the magnetic moment of the “heavy” mode with the extremum in the weak field is, at least, several times greater than the moment of the “light” mode and should be attributed to the magnetosome chains fixed on the bacterial cytoskeleton. The “heavy” fraction also exhibits two orders of magnitude of lower saturation magnetization and the number of magnetic centers for the entire ensemble of the bacteria in the sample, compared to the “light” fraction. This suggests that it is energetically unfavorable for the cells to synthesize a pool of the “heavy” fraction of magnetosomes, due to losses in magnetostatic energy. Only one chain is synthesized in every cell [1–5], as illustrated by the TEM image of Figure 2. This chain is bound to the cytoskeleton to avoid its rolling up. In contrast, the “light” fragments are free to roll up or to couple antiferromagnetically with each other by dipolar forces to minimize their magnetostatic energy. This explains the mean magnetic moments of the “light” fractions being only of the order $10^4 \mu_B$, corresponding to the effective NP size of less than 10 nm, which is much smaller than expected for magnetosomes [1–5,45]. The high concentration of magnetosomes in the “light” fraction can be seen in the AFM image of Figure S1. This fraction with the wide distribution of magnetic moments can probably include, at least partially, nascent (immature) magnetosomes formed after the cell division, the iron-carrying proteins for synthesis, and fragments of the chains formed in dead cells after the destruction of their membranes. These structures can be expected to have significantly smaller moments than that of the magnetosome chain of mature cells. The fragments of the magnetosome chain that are not bound to the cell membrane are probably structurally compacted due to dipolar correlations of the antiferromagnetic type to decrease the magnetostatic energy, resulting in the decrease of their total magnetic moment. The “old” and “new” specimens exhibit more or less close parameters, except only \tilde{M} for MSR-1. The parameters for SO-1 “new” could not be resolved. These peculiarities evidence the possibility of noticeable evolution of even the formalin-fixed culture during one year of storage.

Panels (c) and (f) of Figures 3–6 show M_2 signals recorded at $F_{sc} = 0.02$ Hz with a relatively small hysteresis and close amplitudes in both samples, “old” and “new”, for all strains. Only the amplitude of the response of the “old” sample of the MSR-1 strain somewhat exceeds the average level. Well-defined extrema of the signals located near $H = 0$ correspond to a large moment of the magnetic centers and can be attributed to the “heavy” fraction. However, as the fitting results show, the response also contains a comparable contribution from the “light” fraction with an extremum at $H \sim 10$ kA/m. The increase of F_{sc} to 8 Hz is accompanied by an increase of the hysteresis and, in most samples, by a

shift in the position of the signal extremum from the region $H < 0$ to the region $H > 0$ in the direct scan curves, as Figures 3a, 4a,d, 5a,d, and 6a show. This indicates the large relaxation time, so that the scan period at 8 Hz is too short for the magnetosome ensemble to reach the thermal equilibrium. A considerable increase of the hysteresis in the response of the “old” samples after the one-year storage may be associated with the enlargement of some part of magnetosomes of the “light” fraction, due to fusion of their magnetic cores during the destruction of their lipid shells.

From Table 1, the magnetic moments of the “heavy” fraction vary significantly in different MTB strains. Their values correspond, at most, to the NP size of 25 nm, which is too small for any MTB known [9,45]. The reason is the field hysteresis in the M_2 response, which smears the signal to be processed when averaging between the direct and reverse scans (Equation (8)). As a result, in the vicinity of $H = 0$, the fit curves cannot describe the fast growth of the true signals (Figures 3–5 and 6c,f), and the magnetic moment of the “heavy” fraction turned out to be essentially underestimated. This rapid growth of the signals, both in forward and backward scans, can be fairly well described by the response curves simulated for the magnetic moment $M = 1.7 \cdot 10^6 \mu_B$ (hatched peaks in the vicinity of $H = 0$ in Figures 3f, 4c, and 5f) corresponding to the NP size of 40 nm, which is within the range that is typical for magnetosomes [1–5,9,45,46]. However, magnetosomes form linear chains consisting of dozens of NPs strongly coupled by dipolar forces, and their total magnetic moment is, at least, an order of magnitude larger. The simulation of the nonlinear response from such an array yields a narrow peak centered at $H = 100$ A/m (not shown), well inside the hysteresis region (± 1 kA/m). Thus, for the obtained anisotropy energy of the order 10^3 K, even at the smallest scan frequency used, the low-frequency magnetization dynamics of the array with such a great magnetic moment is still far beyond the SPM regime, and the formalism based on the FP equation may not be applied. To correctly measure this signal, a scan frequency F_{sc} much lower than 0.02 Hz is needed, yet it is unavailable in the setup used. Its upgrade is intended.

3.4. EMR Results

To minimize dielectric losses from the cultivation medium, the samples in a flat cylindrical cuvette 0.15 mm high with a diameter of 20 mm, filled and sealed under nitrogen, were placed at the bottom of a balanced cylindrical resonator with the TE₁₁₁ microwave oscillation type used in the spectrometer [38]. EMR spectra were obtained from the suspensions of BB-1, MSR-1, and AMB-1 strains of the genus *Magnetospirillum*; the spin induction signals were recorded at room temperature. The phase of the reference voltage of the microwave detector was determined from the shape of the signal from the witness sample (nitroxyl radical). The latter was placed on the wall of the microwave cavity opposite the bottom of the resonator with the sample cuvette to avoid the contribution of the sample magnetization to the field at the place of the witness. The EMR signal proportional to the mixture of the dispersion χ''_{yx} - and absorption χ'_{yx} parts of the magnetic susceptibility was registered as a function of the magnetic field ranging from 70 to 520 kA/m. The adjustable mixing angle was preset in the measurement and further specified in the fit procedure.

The suspension of bacteria with magnetosomes, due to their random orientation, is magnetically similar to a polycrystalline ferromagnet. The optical density of the suspensions was measured to be 0.06–0.09, indicating a rather low concentration of the bacteria. Therefore, one may neglect the magnetic interactions between them and consider the bacteria ensemble within the model of independent “grains”. In the case of conventional uniaxial magnetic anisotropy, the signal from nanoparticles of the same type is split into two peaks [47].

In our case, the original EMR signal was registered, rather than its derivative. The initial processing of the spectra consisted in subtracting the background signal from the resonator without a sample. The latter includes the Hall effect from conduction electrons of the resonator material, which are involved in the microwave currents flowing through the bottom of the resonator. Like the resonant magnetic transition in the sample, the Hall effect leads to rotation of the polarization plane of microwave oscillations in the resonator [38]. The Hall effect can

also be observed in the sample if it contains charged carriers. It is known that the line shape of the signal from a polycrystalline ferromagnetic sample is not Lorentzian [47]. Therefore, for the semi-quantitative analysis of the recorded EMR spectra, the line shape of any signal was assumed to be Gaussian. Depending on the number of extrema, two, three, or four Gaussians were used at the fitting, together with the linear Hall signal. Then, for clarity, the Hall signal was subtracted from the fitted spectra. The signals for BB-1, MSR-1, and AMB-1 and their fits are presented in Figure 7. The fit parameters are shown in Table 2.

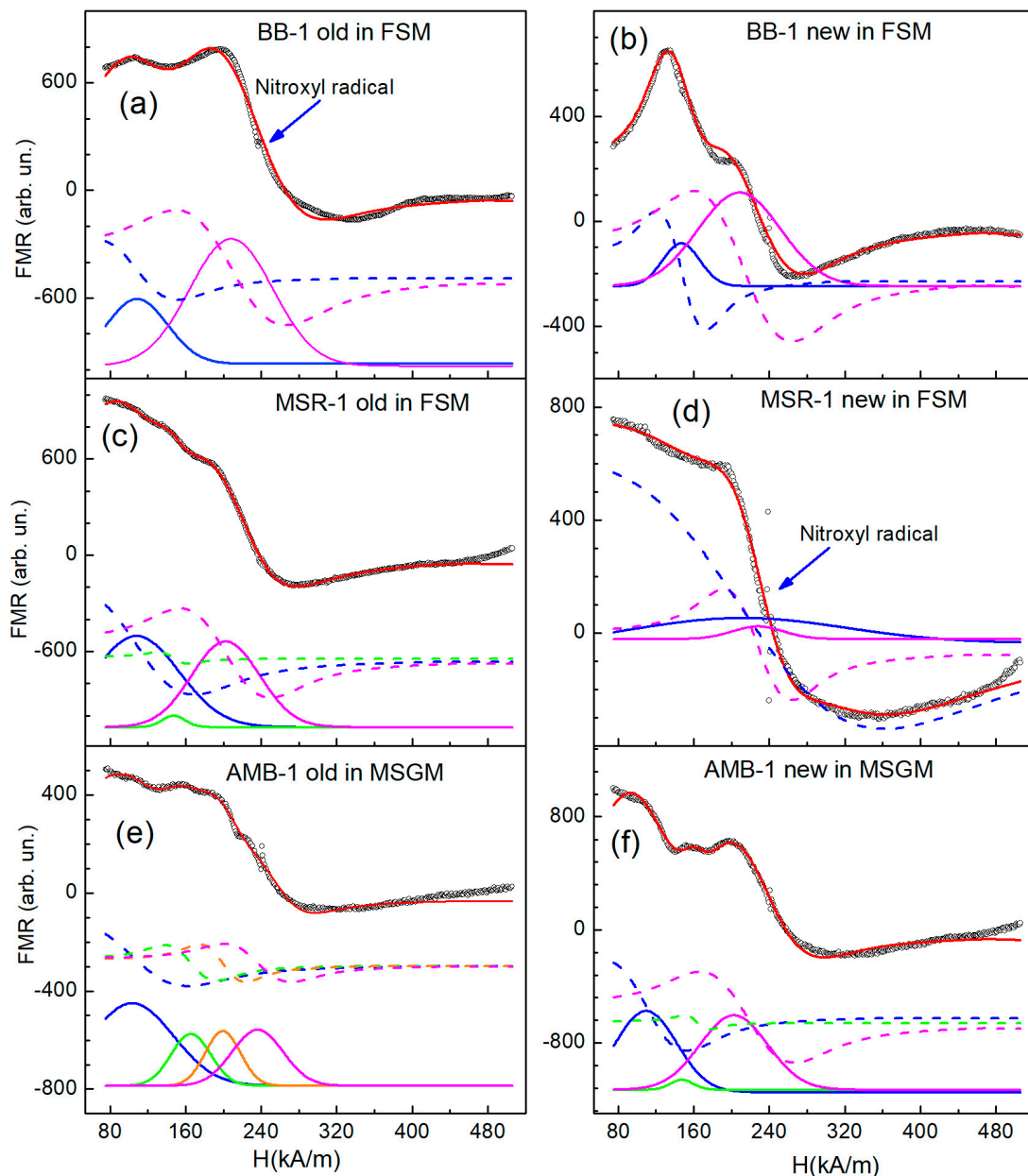


Figure 7. Electron magnetic resonance spectra and their fits for suspensions of BB-1, MSR-1, and AMB-1 strains of the genus *Magnetospirillum*. The experimental signals and the fitting curves are presented by open circles and red lines, respectively. The Gaussians obtained at fitting include both absorption and dispersion (solid and dashed lines, respectively); their contribution to fitting curves with appropriate weights is shown below the experimental points. Referring to Table 1, magenta, blue, green and orange lines represent Gaussians 1, 2, 3, and 4, respectively. The arrows on panels (a,d) indicate the position of the residual signal from the witness (nitroxyl radical, g -factor = 2.0055), after subtracting the background signal from the resonator without the sample.

Table 2. Room temperature fit parameters of EMR spectra lines for *Magnetospirillum* BB-1, MSR-1, and AMB-1 strains.

| Parameters | BB-1 in FSM New | BB-1 in FSM Old | MSR-1 in FSM New | MSR-1 in FSM Old | AMB-1 in MSGM New | AMB-1 in MSGM Old |
|---------------------------|-----------------|-----------------|------------------|------------------|-------------------|-------------------|
| Mixing angle, grad | −66 (1) | −36 (4) | −82 (7) | −40 (2) | −41 (4) | −29 (5) |
| Gaussian 2 | | | | | | |
| g-factor | 3.388 (3) | 4.574 (3) | 2.354 (7) | 4.6 (1) | 4.54 (2) | 4.80 (9) |
| Line width Γ , A/m | 11.58 (4) | 18.9 (1.1) | 64.8 (2.6) | 26.7 (1.4) | 19.0 (9) | 25.5 (2.8) |
| Amplitude, arb.un. | 77 (1) | 189 (33) | 470 (60) | 441 (30) | 320 (34) | 230 (35) |
| Gaussian 1 | | | | | | |
| g-factor | 2.348 (3) | 2.384 (1) | 2.183 (1) | 2.456 (7) | 2.294 (9) | 2.104 (2) |
| Line width Γ , A/m | 23.24 (24) | 25.8 (5) | 16.2 (6) | 20.4 (4) | 22.3 (5) | 15.9 (1.6) |
| Amplitude, arb.un. | 134 (2) | 262 (6) | 55 (4) | 176 (10) | 197 (4) | 42 (19) |
| Gaussian 3 | | | | | | |
| g-factor | | | | 3.376 (4) | 3.04 (1) | 3.00 (4) |
| Line width Γ , A/m | | | | 7.2 (6) | 6.2 (8) | 12.4 (1.8) |
| Amplitude, arb.un. | | | | 11 (2) | 11 (2) | 44 (16) |
| Gaussian 4 | | | | | | |
| g-factor | | | | | | 2.49 (2) |
| Line width Γ , A/m | | | | | | 10.9 (1.1) |
| Amplitude, arb.un. | | | | | | 34 (13) |

Our previous experiments with colloidal aqueous solutions of magnetite nanoparticles in a dextran shell with the average magnetic core size 10 nm and the average magnetic moment $2.6 \times 10^4 \mu_B$ showed the formation of MNP aggregates with the average number of MNPs 55. Due to the minimization of magnetostatic energy by dipolar forces, both of a single aggregate and the entire ensemble of MNPs, the average magnetic moment of the aggregate was only about two moments of a single MNP. The EMR measurements showed a break in these magnetic correlations in an external magnetic field of 110 kA/m [26]. The estimation of the dipolar field created by a magnetosome at the neighboring one in the chain (in the “heavy” fraction), based on the estimated magnetosome moment of $1.7 \times 10^6 \mu_B$ and the average distance between magnetosome centers in the TEM images of 40–50 nm (Figure 1), yields the crossover field $H_{\text{cross}} \approx 250\text{--}350$ kA/m. This means that each magnetosome follows the external field independently in the fields above H_{cross} . The analyzed extrema in the EMR spectra are localized in the lower fields (Figure 7) and arise from magnetosomes that are ferromagnetically linked in the chains by dipolar forces. Since the dipolar correlations in the “light” fraction have, at least partly, an antiferromagnetic character, the magnetic moment of the “light” fraction is an order of magnitude smaller than that of the “heavy” one (Table 1). Therefore, the broad weak signal from the highly dispersed “light” fraction is not actually observed against the background of the signal from the “heavy” fraction with much larger moment. This suggests that the observed EMR signals should be attributed to the “heavy” fraction, whose magnetosome chain is attached to the membrane [1–5,29].

As shown in Figure 7, the amplitudes of the experimental signals for the “old” and “new” fractions differ little for different strains. At the same time, the signal from the “old” fraction is somewhat less than that from the “new” fraction for one and the same strain. The positions of the first of two main fitting signals (magenta Gaussians) near g -factor 2 are practically the same for all strains, BB-1, MSR-1, and AMB-1, both for the “new” and “old” samples, as also shown in Table 2. Hereafter, the g -factor refers to the effective g -factor characterizing the position of the signal in the magnetic field. The closest values of the first Gaussian g -factors in the “new” and “old” samples are found in the AMB-1 strain, while some difference is observed in the BB-1 strain, and some more difference is found in the MSR-1 strain. As for the second main fitting signals (blue Gaussians), their field positions are rather close for all the strains in the sample “old”, while the positions of the second Gaussians are noticeably different in the trials “new”.

In a magnetosome chain, one can expect the orientation of the moments of magnetic core and, probably, their anisotropy axes along the chain due to their dipolar correlations,

providing an additional contribution to the anisotropy. As briefly discussed above, in the case of uniaxial anisotropy, one would expect the EMR signal from the *Magnetospirillum* ensemble to split into two peaks. For the positive anisotropy constant, the second peak is shifted toward weaker fields [47], as it is really observed for the main (magenta and blue) peaks of the “old” and “new” samples in all the strains, with the exception of the MSR-1 “new” one (Figure 7e). In the latter case, both lines exhibit close g -factors, suggesting a rather small magnetic anisotropy.

A comparison of the g -factors of the second main peak (see Table 2 and Figure 7, blue lines) for the “new” and “old” samples of BB-1, MSR-1, and AMB-1 strains shows their increase in the “old” samples for all the strains. In AMB-1, this increase is relatively small compared to the larger increase observed in BB-1 and the maximal increase in MSR-1 (Figure 7c,d and Table 2), suggesting the corresponding increase in magnetic anisotropy in these strains when stored after fixation with 5% formalin.

Note the appearance of an additional weak peak in the EMR spectrum of the “old” sample of the MSR-1 strain, its position being between the main peaks (Figure 7c). In addition, note the appearance of the third weak peak in the spectrum of the “new” sample of the AMB-1 strain, accompanied by one more (the fourth peak) in the signal of the “old” sample of this strain; the positions of the additional peaks are between the main ones as well (Figure 7e,f and Table 2). This indicates different stability of the magnetosome chain in different strains and suggests the decrease of the magnetic anisotropy of the “heavy” fraction chain in parts of the bacterial ensembles. This can be caused by several factors: (i) the presence of cells at different stages of division with different lengths of magnetosome chains and different sizes of immature and mature magnetosomes; (ii) the shortening of the magnetosome chain, due to its partial degradation; and (iii) the folding of magnetosome chains when detached from the cytoskeletons of the cells, accompanied by decreasing both their magnetic moments and the contribution to magnetic anisotropy due to “antiferromagnetic” dipolar correlations. The gradual destruction of magnetosome chains in the “old” samples of some strains at long-term storage occurred not randomly, as evidenced by the appearance of additional peaks with definite g -factors. Otherwise, the random destruction of the magnetosome chains would have resulted in a smeared signal, due to the continuous distribution of g -factors and anisotropy energies.

The result of the evolution of the magnetosome organization in *Magnetospirillum* spp. after the long-term storage can be seen from the AFM data for the BB-1 strain in Figure S1.

4. Conclusions

Magnetosomes produced by six MTB strains of the genus *Magnetospirillum*, BB-1, MSR-1, SO-1, AMB-1, SP-1, and LBB-42, were studied by second-harmonic nonlinear response. Each culture was measured after fixation by 5% formalin, both as-prepared and one year after preparation. A bimodal size and, correspondingly, magnetic moment distribution was found in all the species. The “heavy”, monodisperse mode is suggested to correspond to the fixed-in-space linear chains of magnetosomes in accordance with the transmission electron microscopy data for mature cells of two strains, SO-1 and SP-1. The cell ensemble includes dividing cells at different stages of maturation, which contribute to the signals of both the “light” and “heavy” fractions. The “light”, highly disperse, mode is implied to consist of more or less free shorter fragments. The latter are either rolled up or coupled with each other by dipolar forces to decrease the magnetostatic energy and the magnetic moment of the aggregate. From the AFM image, one can suggest degradation of a part of the cells at long-term storage of the BB-1 culture, even when fixed by formalin. The obtained mean magnetic moments, the saturation magnetizations, and the number of magnetic centers responsible for the signals noticeably differ for all the strains. The “heavy”-fraction parameters are only rough estimations, due to magnetic hysteresis in the M_2 response. Electron magnetic resonance evidenced uniaxial magnetic anisotropy of the “heavy”-fraction magnetosome chains and its different stability in different strains.

Slow destruction of magnetosome chains at long-term storage occurred in certain places, not randomly.

The magnetic parameters were extracted solely from the NLR-M2 measurements, while the EMR data were analyzed phenomenologically to obtain qualitative information on the MTB strains complementing the quantitative data.

Supplementary Materials: The following supporting information can be downloaded at: <https://www.mdpi.com/article/10.3390/app13042431/s1>. Supplementary Figure S1: The AFM image of the *M. moscoviense* BB-1 “old” fixed by addition of 5% formalin to culture after a year of storage.

Author Contributions: Conceptualization, V.R., M.S. and K.G.; methodology, V.R. and V.D.; software, V.D. and I.L.; validation, M.S., D.G. and V.K.; formal analysis, V.D.; investigation, V.R., I.K. and Y.M.; resources, D.G., V.K., N.S. and T.Z.; data curating, V.D. and I.L.; writing—original draft preparation, V.R. and V.D.; writing—review and editing, M.S., K.G. and T.Z.; project administration, M.S. and K.G.; funding acquisition, M.S. and Y.M. All authors have read and agreed to the published version of the manuscript.

Funding: This research was funded by the Ministry of Science and Higher Education of the Russian Federation (Agreement No. 075-15-2022-301 from 20.04.2022), by Russian Science Foundation grant No. 23-25-00273 (<https://rscf.ru/project/23-25-00273/>) magnetic measurements, studies by atomic force microscopy, and data processing were supported. The production of magnetosomes was partially supported by the Russian Federal Academic Leadership Program Priority 2030.

Institutional Review Board Statement: Not applicable.

Informed Consent Statement: Not applicable.

Data Availability Statement: The data that support the finding of this research are not publicly available, due to confidentiality constraints.

Acknowledgments: The authors are grateful to the staff of the PNPI PIK Data Centre for its valuable technical assistance.

Conflicts of Interest: The authors declare no conflict of interest.

References

1. Faivre, D.; Schueler, D. Magnetotactic bacteria and magnetosomes. *Chem. Rev.* **2008**, *108*, 4875–4898. [[CrossRef](#)] [[PubMed](#)]
2. Lefevre, C.; Bernadac, A.; Yu-Zhang, K.; Pradel, N.; Wu, L.-F. Isolation and characterization of a magnetotactic bacterial culture from the Mediterranean Sea. *Environ. Microbiol.* **2009**, *11*, 1646–1657. [[CrossRef](#)] [[PubMed](#)]
3. Lower, B.H.; Bazylinski, D.A. The Bacterial Magnetosome: A Unique Prokaryotic Organelle. *Microb. Physiol.* **2013**, *23*, 63–80. [[CrossRef](#)] [[PubMed](#)]
4. Jacob, J.J.; Suthindhiran, K. Magnetotactic bacteria and magnetosomes—Scope and challenges. *Mater. Sci. Eng. C* **2016**, *68*, 919–928. [[CrossRef](#)]
5. Gareev, K.G.; Grouzdev, D.S.; Kharitonov, P.V.; Kostrov, A.; Koziyeva, V.V.; Sergienko, E.S.; Shevtsov, M.A. Magnetotactic Bacteria and Magnetosomes: Basic Properties and Applications. *Magnetochemistry* **2021**, *7*, 86. [[CrossRef](#)]
6. Alphandery, E.; Guyot, F.; Chebbi, I. Preparation of chains of magnetosomes, isolated from *Magnetospirillum magneticum* strain AMB-1 magnetotactic bacteria, yielding efficient treatment of tumors using magnetic hyperthermia. *Int. J. Pharm.* **2012**, *434*, 444–452. [[CrossRef](#)]
7. Alphandery, E. Applications of Magnetosomes Synthesized by Magnetotactic Bacteria in Medicine. *Front. Bioeng. Biotechnol.* **2014**, *2*, 5. [[CrossRef](#)] [[PubMed](#)]
8. Hergt, R.; Hiegele, R.; Zeisberger, M.; Schüler, D.; Heyen, U.; Hilger, I.; Kaiser, W.A. Magnetic properties of bacterial magnetosomes as potential diagnostic and therapeutic tools. *J. Magn. Magn. Mater.* **2005**, *293*, 80–86. [[CrossRef](#)]
9. Kahani, S.A.; Yagini, Z. A Comparison between Chemical Synthesis Magnetite Nanoparticles and Biosynthesis Magnetite. *Bioinorg. Chem. Appl.* **2014**, *2014*, 384984. [[CrossRef](#)] [[PubMed](#)]
10. Nishio, K.; Ikeda, M.; Gokon, N.; Tsubouchi, S.; Narimatsu, H.; Mochizuki, Y.; Sakamoto, S.; Sandhu, A.; Abe, M.; Handa, H. Preparation of size-controlled (30–100 nm) magnetite nanoparticles for biomedical applications. *J. Magn. Magn. Mater.* **2007**, *310*, 2408–2410. [[CrossRef](#)]
11. Monteil, C.; Grouzdev, D.S.; Perrière, G.; Alonso, B.; Rouy, Z.; Cruveiller, S.; Ginet, N.; Pignol, D.; Lefevre, C.T. Repeated horizontal gene transfers triggered parallel evolution of magnetotaxis in two evolutionary divergent lineages of magnetotactic bacteria. *ISME J.* **2020**, *14*, 1783–1794. [[CrossRef](#)] [[PubMed](#)]

12. Koziava, V.V.; Rusakova, S.A.; Slobodova, N.V.; Uzun, M.; Kolganova, T.V.; Skryabin, K.G.; Grouzdev, D.S. *Magnetospirillum kuznetsovii* sp. nov., a novel magnetotactic bacterium isolated from a lake in the Moscow region. *Int. J. Syst. Evol. Microbiol.* **2019**, *69*, 1953–1959. [CrossRef] [PubMed]
13. Dziuba, M.; Koziava, V.; Grouzdev, D.; Burganskaya, E.; Baslerov, R.; Kolganova, T.; Chernyadyev, A.; Osipov, G.; Andrianova, E.; Gorlenko, V.; et al. *Magnetospirillum caucaseum* sp. nov., *Magnetospirillum marisnigri* sp. nov. and *Magnetospirillum moscoviense* sp. nov., freshwater magnetotactic bacteria isolated from three distinct geographical locations in European Russia. *Int. J. Syst. Evol. Microbiol.* **2016**, *66*, 2069–2077. [CrossRef] [PubMed]
14. Taoka, A.; Kiyokawa, A.; Uesugi, C.; Kikuchi, Y.; Oestreicher, Z.; Morii, K.; Eguchi, Y.; Fukumori, Y. Tethered Magnets Are the Key to Magnetotaxis: Direct Observations of *Magnetospirillum magneticum* AMB-1 Show that MamK Distributes Magnetosome Organelles Equally to Daughter Cells. *Mbio* **2017**, *8*, e00679-17. [CrossRef]
15. Toro-Nahuelpan, M.; Müller, F.D.; Klumpp, S.; Plitzko, J.M.; Bramkamp, M.; Schüler, D. Segregation of prokaryotic magnetosomes organelles is driven by treadmilling of a dynamic actin-like MamK filament. *BMC Biol.* **2016**, *14*, 88. [CrossRef]
16. Wan, J.; Monteil, C.L.; Taoka, A.; Ernie, G.; Park, K.; Amor, M.; Taylor-Cornejo, E.; Lefevre, C.T.; Komeili, A. McaA and McaB control the dynamic positioning of a bacterial magnetic organelle. *Nat. Commun.* **2022**, *13*, 5652. [CrossRef]
17. Marcano, L.; García-Prieto, A.; Muñoz, D.; Barquín, L.F.; Orue, I.; Alonso, J.; Muela, A.; Fdez-Gubieda, M. Influence of the bacterial growth phase on the magnetic properties of magnetosomes synthesized by *Magnetospirillum gryphiswaldense*. *Biochim. Biophys. Acta (BBA) Gen. Subj.* **2017**, *1861*, 1507–1514. [CrossRef] [PubMed]
18. Moisescu, C.; Ardelean, I.I.; Benning, L.G. The effect and role of environmental conditions on magnetosome synthesis. *Front. Microbiol.* **2014**, *5*, 49. [CrossRef] [PubMed]
19. Gandia, D.; Marcano, L.; Gandarias, L.; Villanueva, D.; Orue, I.; Abrudan, R.M.; Valencia, S.; Rodrigo, I.; García, J.; Muela, A.; et al. Tuning the Magnetic Response of *Magnetospirillum magneticum* by Changing the Culture Medium: A Straightforward Approach to Improve Their Hyperthermia Efficiency. *ACS Appl. Mater. Interfaces* **2022**, *15*, 566–577. [CrossRef] [PubMed]
20. Popa, R.; Fang, W.; Nealon, K.H.; Souza-Egipsy, V.; Berquó, T.S.; Benerjee, S.K.; Penn, L.R. Effect of oxidative stress on the growth of magnetic particles in *Magnetospirillum magneticum*. *Int. Microbiol.* **2009**, *12*, 49–57. [PubMed]
21. Firlar, E.; Perez-Gonzalez, T.; Olszewska, A.; Faivre, D.; Prozorov, T. Following iron speciation in the early stages of magnetite magnetosome biomineralization. *J. Mater. Res.* **2016**, *31*, 547–555. [CrossRef]
22. Le Nagard, L.; Zhu, X.; Yuan, H.; Benzerara, K.; Bazylinski, D.A.; Fradin, C.; Besson, A.; Swaraj, S.; Stanescu, S.; Belkhou, R.; et al. Magnetite magnetosome biomineralization in *Magnetospirillum magneticum* strain AMB-1: A time course study. *Chem. Geol.* **2019**, *530*, 119348. [CrossRef]
23. Alphandéry, E.; Ngo, A.T.; Lefèvre, C.; Lisiecki, I.; Wu, L.F.; Pileni, M.P. Difference between the Magnetic Properties of the Magnetotactic Bacteria and Those of the Extracted Magnetosomes: Influence of the Distance between the Chains of Magnetosomes. *J. Phys. Chem. C* **2008**, *112*, 12304–12309. [CrossRef]
24. Gareev, K.G.; Grouzdev, D.S.; Kharitonov, P.V.; Kirilenko, D.A.; Kostrov, A.; Koziava, V.V.; Levitskii, V.S.; Multhoff, G.; Nepomnyashchaya, E.K.; Nikitin, A.V.; et al. Magnetic Properties of Bacterial Magnetosomes Produced by *Magnetospirillum caucaseum* SO-1. *Microorganisms* **2021**, *9*, 1854. [CrossRef]
25. Lazuta, A.V.; Ryzhov, V.A.; Runov, V.V.; Khavronin, V.P.; Deriglazov, V.V. Temperature evolution of superparamagnetic clusters in single-crystal La_{0.85}Sr_{0.15}CoO₃ characterized by nonlinear magnetic ac response and neutron depolarization. *Phys. Rev. B* **2015**, *92*, 14404–14411. [CrossRef]
26. Ryzhov, V.A.; Kiselev, I.A.; Smirnov, O.P.; Chernenkov, Y.P.; Deriglazov, V.V.; Marchenko, Y.Y.; Yakovleva, L.Y.; Nikolaev, B.P.; Bogachev, Y.V. Comprehensive characterization of magnetite-based colloid for biomedical applications. *Appl. Phys. A* **2019**, *125*, 322. [CrossRef]
27. Schleifer, K.H.; Schüler, D.; Spring, S.; Weizenegger, M.; Amann, R.; Ludwig, W.; Köhler, M. The Genus *Magnetospirillum* gen. nov. Description of *Magnetospirillum gryphiswaldense* sp. nov. and Transfer of *Aquaspirillum magnetotacticum* to *Magnetospirillum magnetotacticum* comb. nov. *Syst. Appl. Microbiol.* **1991**, *14*, 379–385. [CrossRef]
28. Heyen, U.; Schüler, D. Growth and magnetosome formation by microaerophilic *Magnetospirillum* strains in an oxygen-controlled fermentor. *Appl. Microbiol. Biotechnol.* **2003**, *61*, 536–544. [CrossRef]
29. Matsunaga, T.; Sakaguchi, T.; Tadakoro, F. Magnetite formation by a magnetic bacterium capable of growing aerobically. *Appl. Microbiol. Biotechnol.* **1991**, *35*, 651–655. [CrossRef]
30. Yang, C.-D.; Takeyama, H.; Tanaka, T.; Matsunaga, T. Effects of growth medium composition, iron sources and atmospheric oxygen concentrations on production of luciferase-bacterial magnetic particle complex by a recombinant *Magnetospirillum magneticum* AMB-1. *Enzym. Microb. Technol.* **2001**, *29*, 13–19. [CrossRef] [PubMed]
31. Gullity, B.D.; Graham, C.D. *Introduction to Magnetic Materials*, 2nd ed.; John Wiley & Sons: New York, NY, USA, 2009; pp. 359–397.
32. Ryzhov, V.A.; Larionov, I.I.; Fomichev, V.N. On the spurious signal in the longitudinal nonlinear susceptibility of magnets at the second harmonic of excitation frequency. *Tech. Phys.* **1996**, *41*, 620–626.
33. Ryzhov, V.A.; Zavatskii, E.I. Device to Research Magnetic Properties of Magnetics. Russian Federation Patent 2,507,527, 20 February 2014. Available online: <https://patents.google.com/patent/RU2507527C1/en?q=RU2507527> (accessed on 10 February 2023).
34. Shevtsov, M.A.; Nikolaev, B.P.; Ryzhov, V.A.; Yakovleva, L.Y.; Dobrodumov, A.V.; Marchenko, Y.Y.; Margulis, B.A.; Pitkin, E.; Guzhova, I.V. Brain tumor magnetic targeting and biodistribution of superparamagnetic iron oxide nanoparticles linked with 70-kDa heat shock protein study by nonlinear longitudinal response. *J. Magn. Magn. Mater.* **2015**, *388*, 123–134. [CrossRef]

35. Lazuta, A.V.; Larionov, I.I.; Ryzhov, V.A. Second-harmonic response of a cubic ferrromagnet in the critical paramagnetic neighborhood of TC. *Sov. Phys. JETP* **1991**, *73*, 1086–1095.
36. Ryzhov, V.A.; Pleshakov, I.V.; Nechitailov, A.; Glebova, N.V.; Pyatyshev, E.N.; Malkova, A.V.; Kiselev, I.A.; Matveev, V. Magnetic Study of Nanostructural Composite Material Based on Cobalt Compounds and Porous Silicon. *Appl. Magn. Reson.* **2014**, *45*, 339–352. [[CrossRef](#)]
37. Ryzhov, V.A.; Multhoff, G.; Shevtsov, M.A. Detection of Magnetosome-Like Structures in Eukaryotic Cells Using Nonlinear Longitudinal Response to ac Field. *Appl. Magn. Reson.* **2019**, *50*, 943–957. [[CrossRef](#)]
38. Ryzhov, V.A.; Zavatskii, E.I.; Solov'ev, V.A.; Kiselev, I.A.; Fomichev, V.N.; Bikineev, V.A. Spectrometer for studying broad dipole transitions in magnets and the Hall conductivity at microwave frequencies in conducting materials. *Tech. Phys.* **1995**, *40*, 71–78.
39. Ryzhov, V.A.; Lazuta, A.V.; Smirnov, O.P.; Kiselev, I.A.; Chernenkov, Y.P.; Borisov, S.A.; Troaynchuk, I.O.; Khalyavin, D.D. Neutron diffraction, magnetization, and ESR studies of pseudocubic Nd_{0.75}Ba_{0.25}MnO₃ and its critical behavior above T_C. *Phys. Rev. B* **2005**, *72*, 134427. [[CrossRef](#)]
40. Yudintceva, N.; Mikhailova, N.; Bobkov, D.; Yakovleva, L.; Nikolaev, B.; Krasavina, D.; Muraviov, A.; Vinogradova, T.; Yablonskiy, P.; Samusenko, I.; et al. Evaluation of the Biodistribution of Mesenchymal Stem Cells in a Pre-clinical Renal Tuberculosis Model by Non-linear Magnetic Response Measurements. *Front. Phys.* **2021**, *9*, 625622. [[CrossRef](#)]
41. Bedanta, S.; Kleemann, W. Supermagnetism. *J. Phys. D Appl. Phys.* **2008**, *42*, 013001. [[CrossRef](#)]
42. Lohße, A.; Borg, S.; Raschdorf, O.; Kolinko, I.; Tompa, É.; Pósfai, M.; Schüler, D. Genetic dissection of the mamAB and mms6 operons reveals a gene set essential for magnetosome biogenesis in *Magnetospirillum gryphiswaldense*. *J. Bacteriol.* **2014**, *196*, 2658–2669. [[CrossRef](#)]
43. Uebe, R.; Schüler, D. Magnetosome biogenesis in magnetotactic bacteria. *Nat. Rev. Microbiol.* **2016**, *14*, 621–637. [[CrossRef](#)] [[PubMed](#)]
44. Ben-Shimon, S.; Stein, D.; Zarivach, R. Current view of iron biomineralization in magnetotactic bacteria. *J. Struct. Biol. X* **2021**, *5*, 100052. [[CrossRef](#)] [[PubMed](#)]
45. Klumpp, S.; Kiani, B.; Vach, P.; Faivre, D. Navigation with magnetic nanoparticles: Magnetotactic bacteria and magnetic micro-robots. *Phys. Scr.* **2015**, *T165*, 014044. [[CrossRef](#)]
46. Klumpp, S.; Faivre, D. Interplay of Magnetic Interactions and Active Movements in the Formation of Magnetosome Chains. *PLoS ONE* **2012**, *7*, e33562. [[CrossRef](#)] [[PubMed](#)]
47. Gurevich, A.G. *Magnetic Resonance in Ferrites and Antiferromagnets*; "Nauka": Moskow, Russia, 1973; pp. 100–109.

Disclaimer/Publisher's Note: The statements, opinions and data contained in all publications are solely those of the individual author(s) and contributor(s) and not of MDPI and/or the editor(s). MDPI and/or the editor(s) disclaim responsibility for any injury to people or property resulting from any ideas, methods, instructions or products referred to in the content.